Article

Discovery Medicine 2024; 36(190): 2264–2273
https://doi.org/10.24976/Discov.Med.202436190.208

BRIP1 Induced Ferroptosis to Inhibit Glioma Cells and was Associated with Increased Oxidative Stress

Cheng Chen[1,†], Zhong-Hua Wu[2,†], Xiao-Jian Lu[1], Jin-Long Shi[1,*]

[1]Department of Neurosurgery, Affiliated Hospital of Nantong University, Medical School of Nantong University, 226001 Nantong, Jiangsu, China
[2]Department of Neurosurgery, The Sixth People's Hospital of Nantong, 226011 Nantong, Jiangsu, China
*Correspondence: shijlsjwk@163.com (Jin-Long Shi)
[†]These authors contributed equally.
Published: 20 November 2024

Background: Glioma, a malignant brain tumour, poses a significant threat to human life and well-being. Identifying new treatment targets is crucial. This study aimed to explore the impact of *BRIP1* (BRCA1 interacting helicase 1) on glioma cell ferroptosis and its underlying mechanisms.

Methods: We utilized GEPIA (Gene Expression Profiling Interactive Analysis) to predict the expression of *BRIP1* in glioma. The expression of *BRIP1* was evaluated in normal brain glial cell lines (HEB) as well as two glioblastoma (GBM) cell lines (U87 and U251) using qRT-PCR (quantitative RT-PCR) and Western blot analyses. U251 cells were specifically chosen to investigate the impact of *BRIP1* down-regulation and treatment with erastin (a ferroptosis activator) on cell viability and proliferation. In U251 cells, si-*BRIP1* was administered in combination with the necroptosis inhibitor Necrostain-1 (Nec-1), apoptosis inhibitor Z-VAD-FMK (carbobenzoxy-valyl-alanyl-aspartyl- [O-methyl]-fluoromethylketone), autophagy inhibitor CQ (Chloroquine), pyroptosis inhibitor VX765 (Belnacasan), or ferroptosis inhibitor Fer-1 (ferrostain-1), as well as erastin+Fer-1, to determine the mode of programmed cell death using the CCK-8 (Cell counting kit-8) assay. Malondialdehyde (MDA) and glutathione (GSH) levels were measured using ELISA (Enzyme linked immunosorbent assay). Intracellular Fe^{2+} content was detected using a commercial reagent kit. *Gpx4* (Glutathione peroxidase 4) levels were measured using Western blot analysis. The relationship between *BRIP1* and *SLC7A11* (Solute Carrier Family 7 Member 11) was verified by co-IP (co-immunoprecipitation) experiments. The level of *SLC7A11* and *SLC3A2* (Solute Carrier Family 3 Member 2) was analyzed through qRT-PCR and Western blot analyses. A rescue experiment was conducted to observe the effects of *SLC7A11* overexpression on si-*BRIP1*-treated U251 cells.

Results: The GEPIA database predicted that the expression level of *BRIP1* was increased in glioma. The expression level of *BRIP1* was higher in U251 cells compared to HEB and U87 cells ($p < 0.05$). Both down-regulation of *BRIP1* and treatment with erastin resulted in inhibited cell viability and proliferation in U251 cells ($p < 0.05$). The mode of programmed cell death in si-*BRIP1*-treated U251 cells was ferroptosis. Following si-*BRIP1* transfection or erastin treatment, there was an increase in the levels of MDA and intracellular Fe^{2+} content, as well as a decrease in the levels of GSH, *Gpx4*, and *SLC7A11* ($p < 0.05$). However, these alterations observed in the si-*BRIP1* group were reversed by Fer-1 treatment ($p < 0.05$). The co-IP results demonstrated that BRIP1 and SLC7A11 were able to bind to each other. Up-regulation of *SLC7A11* reversed the reduction in cell viability, the increase in MDA, the reduction in GSH, the increase in Fe^{2+} content, and the down-regulation of *Gpx4* in si-*BRIP1*-treated U251 cells ($p < 0.05$).

Conclusion: In this study, we found that down-regulation of *BRIP1* could inhibit cell viability and proliferation in glioma cells through the induction of ferroptosis. This process was associated with increased oxidative stress, which was mediated by the down-regulation of S*LC7A11* (*xCT* (Cysteine/glutamate transporter)) expression.

Keywords: *BRIP1*; ferroptosis; glioma cells; *SLC7A11*; oxidative stress; *Gpx4*

Introduction

Glioma is a brain or spinal cord tumor that develops from glial cells [1]. Human gliomas are categorized based on their origin from specific types of glial cells. The most prevalent classifications include astrocytomas, oligodendrogliomas, and ependymomas [2]. Gliomas can be either benign (non-cancerous) or malignant (cancerous). Among them, high-grade glioblastomas are the most common and aggressive form of primary brain tumors [3]. High-grade glioblastomas exhibit rapid growth, invasiveness into nearby brain tissue, and resistance to treatment [4]. Symptoms of gliomas can vary based on tumor size and location. Common signs may include headaches, seizures, cognitive challenges, behavioral or personality changes, and motor impairments [5]. Diagnosing gliomas typically involves a combination of imaging techniques like MRI (Magnetic Resonance Imaging) or CT (Computed to-

mography) scans. A biopsy is then performed to determine the type and grade of the tumor. Treatment options for gliomas include surgical intervention, radiation therapy, and chemotherapy [6]. Further research is needed to fully understand the underlying mechanisms of malignant gliomas and to explore new therapeutic approaches.

Programmed cell death refers to a series of tightly regulated cellular processes that lead to the death of a cell [7]. It serves important roles in development, tissue homeostasis, immune response, and the elimination of damaged or unwanted cells [8]. Programmed cell death encompasses various types, such as apoptosis, autophagy, necroptosis, ferroptosis, and pyroptosis [9]. Ferroptosis, a recently discovered form of programmed cell death, has attracted considerable interest in tumor research and treatment. It is characterized by the accumulation of lipid peroxides and iron-dependent reactive oxygen species (ROS) [10]. Glutathione peroxidase 4 (*Gpx4*) is a crucial player in ferroptosis, as it functions to safeguard cells against lipid peroxidation, and iron metabolism regulators. Inhibition of *Gpx4* or alterations in iron metabolism can trigger ferroptosis [11]. Ferroptosis has been identified as the predominant form of programmed cell death in glioma, and it has been associated with the induction of immunosuppression and resistance to immunotherapy [12]. Inducing ferroptosis represents a promising avenue for glioma treatment, as ferroptosis-related processes have been implicated in chemoresistance and radioresistance in glioma [13]. A previous study has demonstrated that a gene signature associated with ferroptosis can serve as a prognostic indicator and predict the response to immunotherapy in glioma [14]. Indeed, further research is warranted to explore the potential of ferroptosis as a treatment strategy for glioma.

BRCA1 interacting helicase 1 (*BRIP1*) is a gene that encodes a DNA helicase involved in DNA repair and maintenance of genomic stability [15]. Mutations in the *BRIP1* gene have been linked to an elevated susceptibility to various tumor types, such as breast, ovarian, and pancreatic cancers [16]. These mutations can disrupt the normal function of *BRIP1*, impairing its ability to repair damaged DNA and potentially leading to the accumulation of genetic alterations that contribute to tumor development [17]. However, its role in ferroptosis and glioma biology is still unclear.

Solute Carrier Family 7 Member 11 (*SLC7A11*), also known as *xCT*, is a gene that encodes a subunit of the cystine/glutamate antiporter system [18]. It plays a crucial role in cellular redox balance and antioxidant defense by facilitating the uptake of cystine, which is used for the synthesis of the antioxidant molecule glutathione (GSH) [19]. *SLC7A11* has garnered significant attention due to its involvement in regulating cellular sensitivity to oxidative stress and ferroptosis [20]. *SLC7A11* up-regulation has been observed in different cancer types, including glioma, and is linked to chemoresistance and tumor progression [21]. Hypoxia worsens glioma resistance to sulfasalazine-induced ferroptosis by activating the phosphoinositide 3-kinase (*PI3K*)/protein kinase B (*Akt*)/hypoxia-inducible factor alpha (*HIF-1*α) signaling pathway, causing the up-regulation of *SLC7A11* [22]. However, the regulatory relationship between *BRIP1* and *SLC7A11* (*xCT*) in glioma is not yet clear and requires further research.

In our study, we performed *in vitro* experiments to investigate the impact of *BRIP1* on ferroptosis in glioma cells and to elucidate the regulatory relationship between *BRIP1* and *SLC7A11* (*xCT*).

Material and Methods

Reagents

Specific antibodies against BRIP1 (#4578), Gpx4 (#52455), SLC7A11 (#12691), Solute Carrier Family 3 Member 2 (SLC3A2) (#13180), and β-actin (#4970) were bought from Cell Signaling Technology (CST, Danvers, MA, USA). The Fe^{2+} content detection kit was obtained from Abcam (#ab83366, Cambridge, MA, USA). The Cell counting kit-8 (CCK-8) kit (#C0037), EdU (5-Ethynyl-2′-deoxyuridine) Cell Proliferation Kit (#C0071S), malondialdehyde (MDA) detection kit (#S0131M), GSH detection kit (#S0053), and erastin (#SC0224) were obtained from Beyotime (Beijing, China). Necrostain-1 (Nec-1, #HY-15760), Z-VAD(OH)-FMK (Z-VAD, #HY-16658B), Chloroquine (CQ, #HY-17589A), Belnacasan (VX765, #HY-13205) and ferrostain-1 (Fer-1, #HY-100579) were purchased from MedChem Express (MCE, Monmouth Junction, NJ, USA). All siRNA and plasmids were purchased from Ribobio (#20231016, Guangzhou, China).

Database to Analyze BRIP1 Expression in Human Glioma

We utilized the GEPIA (Gene Expression Profiling Interactive Analysis) database (http://gepia.cancer-pku.cn/) to compare the expression of *BRIP1* between glioma patients and healthy individuals. Briefly, after opening the URL, we typed the word BRIP1 in the search box, then clicked on the EXPRESSION DIY option, selected the GBM (glioblastoma) option in the Datasets Selection and clicked on the Plot button to get the results.

Cell Culture and Treatment

HEB glial cells (#H209) and HEK293T cells (#H237) were obtained from ScienCell (Carlsbad, CA, USA), and U87 (#HTB-14) and U251 (#HTB-15) GBM cell lines were obtained from ATCC (Manassas, VA, USA). HEB cells and HEK293T cells were cultured in DMEM (Dulbecco's modified eagle medium, #10313021, Gibco, Grand Island, NY, USA) with 20% FBS (Fetal Bovine Serum, #10099141C, Gibco, Grand Island, NY, USA) at 37 °C and 5% CO_2. U87 and U251 cells were cultured in DMEM with 10% FBS from Gibco (Grand Island, NY, USA). All cells were identified with STR and tested for mycoplasma.

Next, U251 cells were transfected with si-*BRIP1* using Lipofectamine 2000 (#11668019, Thermo Fisher Scientific, Waltham, MA, USA) or treated with 5 μM erastin for 24 hours at 37 ℃. To clarify the mode of programmed cell death, another *in vitro* experiment was divided into 7 groups: si-*BRIP1* (5′-GGUGCUGUUGUUCUACUAAAC-3′, 50 nM), si-*BRIP1*+Nec-1 (10 μM), si-*BRIP1*+Z-VAD (10 μM), si-*BRIP1*+CQ (25 μM), si-*BRIP1*+VX765 (40 μM), si-*BRIP1*+Fer-1 (1 μM), erastin+Fer-1. To explore the role of BRIP1 in ferroptosis, U251 cells were treated with si-NC (5′-CACGATAAGACAATGTATTT-3′), si-*BRIP1*, erastin or si-*BRIP1*+Fer-1. To further study the regulation between *BRIP1* and *SLC7A11*, U251 cells were treated with si-NC, si-*BRIP1* or si-*BRIP1*+pc-SLC7A11 (2 μg). The pc-SLC7A11 plasmid was constructed by linking the CDS (coding domain sequence) region of SLC7A11 into the pcDNA3.0 plasmid vector. Next, cell functional analysis was performed, and RNA and protein were extracted for quantitative RT-PCR (qRT-PCR) and Western blot analysis, respectively.

Cell Viability

Cells were seeded at a density of 1×10^4 cells per well in a 96-well plate and incubated with DMEM medium at 37 °C in a 5% CO_2 atmosphere. After 24 hours of treatment, cell viability was assessed using a CCK-8 kit (#C0037, Beyotime, Beijing, China). The OD value was analyzed on the Microplate Reader (#1681150, Bio-Rad, Hercules, CA, USA) at 450 nm. Three repeats were conducted in each experiment. Cell viability (%) = [OD value (treated group) – OD value (blank group)]/[OD value (treated control group) – OD value (blank group)] × 100.

EdU Assay

Cells were plated at a density of 1×10^6 per well. After treatment, cells were exposed to 50 μM EdU buffer (#C0071S, Beyotime, Beijing, China) at 37 °C for 120 minutes. Subsequently, cells were fixed with 4% paraformaldehyde (#P0099, Beyotime, Beijing, China) for 30 minutes and permeabilized with 0.1% Triton X-100 (#GC204003, Servicebio, Wuhan, China) for an additional 20 minutes. 4’,6-diamidino-2-phenylindole (DAPI) (#C1002, Beyotime, Beijing, China) staining was used to visualize cell nucleic acids, and images were captured by fluorescence microscope (#CKX53, Nikon, Tokyo, Japan). Cell proliferation rates were quantified using ImageJ software (Version 1.8.0, NIH, Bethesda, MD, USA).

Antioxidant Assay

Antioxidant enzyme activities in cells, including GSH activity and MDA content, were detected using assay kits based on the manufacturer’s instructions.

Measurement of Fe^{2+} Content

Cells were seeded at a density of 1×10^5 cells/mL in a 12-well culture plate. To measure intracellular Fe^{2+} levels, a Ferro-orange kit (#ab83366, Abcam, Cambridge, MA, USA) was used following the manufacturer’s instructions. After treatment, the cells were incubated in serum-free medium for 4 hours and subsequently stained with Ferro-orange for 30 minutes at 37 °C. The fluorescence absorbance of the culture was measured using a microplate spectrophotometer (#1681150, Bio-Rad, Hercules, CA, USA), with specific excitation and emission wavelengths, to quantify the fluorescence intensity.

qRT-PCR

RNA was extracted from cells using Trizol reagent (#R0016, Beyotime, Beijing, China). The isolated RNA was then converted into cDNA using a cDNA synthesis kit (#11119ES60, YEASEN, Shanghai, China). Subsequently, PCR reactions were carried out on the ABI 7900 fluorescence quantitative PCR instrument (#A28137, Thermo Fisher Scientific, Waltham, MA, USA). Primers were as follows: *BRIP1* (human): 5′- CTTACCCGTCACAGCTTGCTA-3′ and 5′-CACTAAGAGATTGTTGCCATGCT-3′, *SLC7A11* (human): 5′-TCTCCAAAGGAGGTTACCTGC-3′ and 5′- AGACTCCCCTCAGTAAAGTGAC-3′, *SLC3A2* (human): 5′-TGAATGAGTTAGAGCCCGAGA-3′ and 5′- GTCTTCCGCCACCTTGATCTT-3′, *GAPDH* (human): 5′-CATCATCCCTGCCTCTACTGG-3′ and 5′-GTGGGTGTCGCTGTTGAAGTC-3′. The expression of the *GAPDH* gene was used as a reference to normalize the mRNA expression levels. The $2^{-\Delta\Delta CT}$ method was employed for relative quantification.

Co-Immunoprecipitation (Co-IP)

For co-IP assays, protein lysates were prepared from HEK293T cells in a buffer containing 50 mM Tris-HCl (pH 7.5, #ST768, Beyotime, Beijing, China), 150 mM NaCl (#ST347, Beyotime, Beijing, China), 0.1% NP-40 (#P0013F, Beyotime, Beijing, China), and a mixture of protease inhibitors (#P8215, Roche, Basel, Switzerland). The lysates were washed with 100 μL of protein A/G agarose beads (#36417ES03, YEASEN, Shanghai, China) in 1 mL lysis buffer. The lysates were then incubated with anti-BRIP1 co-IP antibody (#ab264133, Abcam, Cambridge, MA, USA), or control IgG (#ab205718, Abcam, Cambridge, MA, USA) overnight with the protein A/G agarose beads. The complexes were washed three times with lysis buffer and resuspended in 2× SDS loading buffer (#P0015B, Beyotime, Beijing, China). The immunoprecipitated proteins were eluted from the beads by incubation at 95 °C for 5 min. The eluted proteins were detected by immunoblotting after separation by SDS-PAGE.

Western Blot

Total proteins were extracted from cells using RIPA buffer (#P0013B, Beyotime, Beijing, China). The concentration of the proteins was determined using a commercial kit (#P0009, Beyotime, Beijing, China). Next, 60 µg of proteins were separated using 15% SDS-PAGE and transferred onto a PVDF membrane (#IPVH00005, Merck & Millipore, Billerica, MA, USA). A solution of 5% milk powder in TBST (#28360, Thermo Fisher Scientific, Waltham, MA, USA) was used to block nonspecific binding. The membranes were subsequently incubated overnight at 4 °C with primary antibodies against *BRIP1* (4578, 1:1000), *Gpx4* (52455, 1:1000), *SLC7A11* (12691, 1:1000), *SLC3A2* (13180S, 1:1000), and *β-actin* (4967, 1:3000) (CST, Danvers, MA, USA). After washing with TBST, the membranes were incubated with an HRP-conjugated secondary antibody (A0208, 1:3000, Beyotime, Beijing, China). Protein bands were detected using enhanced chemiluminescence (#WBULP, Fcmacs, Nanjing, China), with β-actin serving as an internal reference for normalization. The protein expression levels were quantified using ImageJ software (Version 1.8.0, NIH, Bethesda, MD, USA). Analytical values were obtained by comparing the grey values of the target protein bands with the grey values of β-actin (internal reference).

Statistical Analysis

SPSS software (Version 22; IBM, Armonk, NY, USA) was used for statistical analysis. Continuous data were presented as means $\pm$ SD. Group comparisons were made using *t*-tests, one-way ANOVA, and LSD tests. p values $<$ 0.05 indicated a significant difference between groups.

Results

The Expression of BRIP1 in Glioma Patients and GBM Cell Lines

In our study, we utilized the GEPIA database, a predictive tool, to estimate the expression level of *BRIP1* in glioma patients and healthy individuals. Our analysis revealed a significant increase in *BRIP1* levels in glioma patients compared to healthy controls (Fig. 1A) ($p < 0.05$). Subsequently, we further investigated the expression of *BRIP1* in HEB, U87, and U251 cell lines using qRT-PCR and Western blot analyses. As depicted in Fig. 1B,C, the expression of *BRIP1* was significantly elevated in U87 and U251 cells compared to HEB cells ($p < 0.05$). Notably, U251 cells exhibited the highest expression level of *BRIP1* among the tested cell lines. Based on these findings, U251 cells were selected as the *in vitro* model for subsequent glioma studies. Consequently, U251 cells were chosen as the preferred *in vitro* model for further glioma research.

The Effects of Down-Regulation of BRIP1 on Cell Viability and Proliferation in U251 Cells

To evaluate the transfection efficiency, we assessed the expression of *BRIP1* using Western blot after transfecting cells with si-NC or si-*BRIP1*. Results demonstrated a significant decrease in *BRIP1* expression in the si-*BRIP1* group compared to the si-NC group (Fig. 2A) ($p < 0.01$). Additionally, we examined cell viability using the CCK-8 assay, which revealed a significant inhibition of cell viability following si-*BRIP1* transfection (Fig. 2B) ($p < 0.001$). Moreover, cell proliferation was evaluated using the EdU assay, which demonstrated a reduction in cell proliferation in the si-*BRIP1* group (Fig. 2C) ($p < 0.01$). These results provide strong evidence that si-*BRIP1* effectively downregulates *BRIP1* expression and influences cell viability and proliferation.

The Effects of Erastin on Cell Viability and Proliferation in U251 Cells

We treated U251 cells with erastin, a well-known ferroptosis activator, to investigate its impact on cell viability and proliferation. The CCK-8 assay and EdU assay were utilized to evaluate these cellular functions. Importantly, erastin treatment significantly reduced both cell viability and proliferation in U251 cells (Fig. 3A,B) ($p < 0.05$). These findings suggest that si-*BRIP1* may have a similar effect to erastin in activating ferroptosis in U251 cells, indicating a potential role of *BRIP1* in regulating ferroptotic processes.

The Effects of Down-Regulation of BRIP1on Ferroptosis in U251 Cells

CCK-8 assay was used to clarify the mode of programmed cell death in U251 cells transfected with si-*BRIP1*. We found that cell viability was not affected after treatment with Nec-1, Z-VAD, CQ, or VX765 in the si-*BRIP1*-treated U251 cells. However, it was increased in si-*BRIP1*+Fer-1 and erastin+Fer-1 groups, indicating that si-*BRIP1* might promote ferroptosis in U251 cells (Fig. 4A) ($p < 0.05$). Next, the levels of GSH and MDA were measured (Fig. 4B). The level of MDA was increased in the si-*BRIP1* and erastin groups ($p < 0.05$), whereas the increase was reversed by Fer-1 in the si-*BRIP1*+Fer-1-treated group ($p < 0.05$). The level of GSH was decreased in the si-*BRIP1* and erastin groups ($p < 0.05$), whereas the decrease was reversed by Fer-1 in the si-*BRIP1*+Fer-1-treated group ($p < 0.05$). We also detected Fe^{2+} in U251 cells. The content of Fe^{2+} was increased in the si-*BRIP1* and erastin groups ($p < 0.05$), whereas the increase was reversed by Fer-1 in the si-*BRIP1*+Fer-1-treated group (Fig. 4C) ($p < 0.05$). To further study the effects of si-*BRIP1* on ferroptosis, we analyzed the expression of *Gpx4* by Western blot. The protein level of Gpx4 was decreased in the si-*BRIP1* and erastin groups ($p < 0.05$), whereas the decrease was reversed by

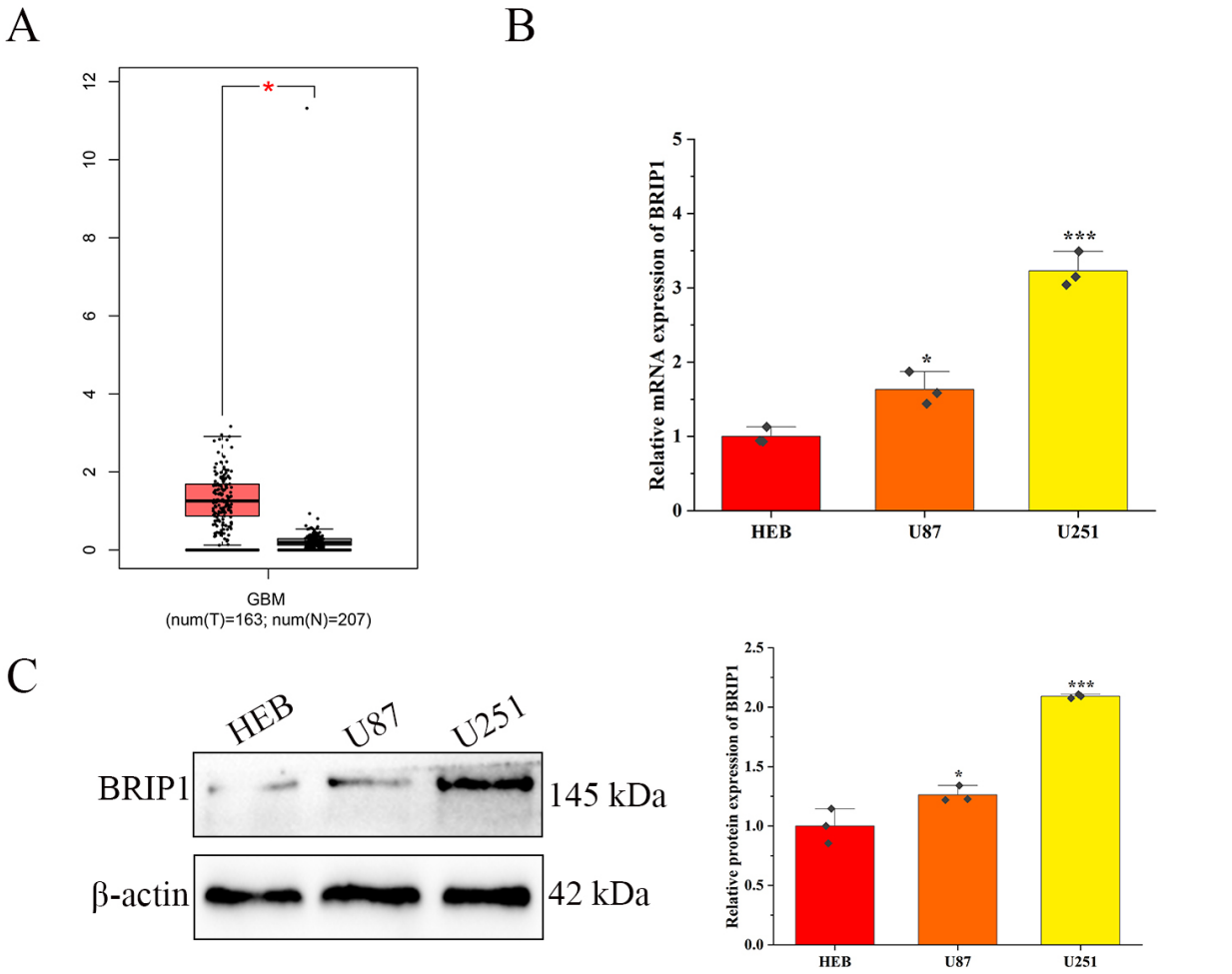

Fig. 1. Expression analysis of BRCA1 interacting helicase 1 (*BRIP1*) in glioma patients and cell lines. (A) Prediction of *BRIP1* expression in glioma patients and healthy controls using the Gene Expression Profiling Interactive Analysis (GEPIA) database. The tumor group is indicated in red and the normal control group in black. (B) Quantitative RT-PCR (qRT-PCR) analysis of *BRIP1* expression in HEB, U87, and U251 cell lines, n = 3. (C) Western blot analysis of BRIP1 protein expression in HEB, U87, and U251 cell lines, n = 3. * $p < 0.05$, *** $p < 0.001$. GBM, glioblastoma.

Fer-1 in the si-*BRIP1*+Fer-1-treated group (Fig. 4D) ($p < 0.05$). Overall, these results indicate that down-regulation of *BRIP1* can activate ferroptosis in U251 cells.

The Effects of Down-Regulation of BRIP1 or Treatment with Erastin on the Expression of SLC7A11 and SLC3A2 in U251 Cells

First, we verified the relationship between BRIP1 and SLC7A11 using co-IP experiments, which showed that BRIP1 and SLC7A11 were able to bind to each other (Fig. 5A). In this study, we examined the expression of *SLC7A11* and *SLC3A2* using qRT-PCR and Western blot analyses (Fig. 5B,C). Interestingly, we did not observe any significant differences in the levels of *SLC3A2* among the different experimental groups. However, we did observe a reduction in *SLC7A11* expression in both the si-*BRIP1* and erastin-treated groups ($p < 0.05$). Importantly, the reduction in *SLC7A11* expression caused by si-*BRIP1* treatment was reversed when Fer-1, a ferroptosis inhibitor, was added ($p < 0.05$). Based on these findings, we decided to further investigate the role of *SLC7A11* in the cellular functions of si-*BRIP1*-treated U251 cells in subsequent experiments.

The Role of SLC7A11 in the Rescue Experiment in si-BRIP1-Treated U251 Cells

To verify transfection efficiency, the expression of *SLC7A11* was analyzed after transfecting with pc-NC or pc-SLC7A11 by Western blot. We found the level of *SLC7A11* was increased in the pc-*SLC7A11* group (Fig. 6A) ($p < 0.01$). The reduction of cell viability induced by si-*BRIP1* was reversed by pc-*SLC7A11* (Fig. 6B) ($p < 0.001$). The decrease in GSH and the increase in MDA caused by si-*BRIP1* treatment was reversed by pc-*SLC7A11* (Fig. 6C) ($p < 0.01$). The increase in Fe^{2+} content and down-regulation of *Gpx4* induced by si-*BRIP1* were reversed by pc-*SLC7A11* (Fig. 6D,E) ($p < 0.01$).

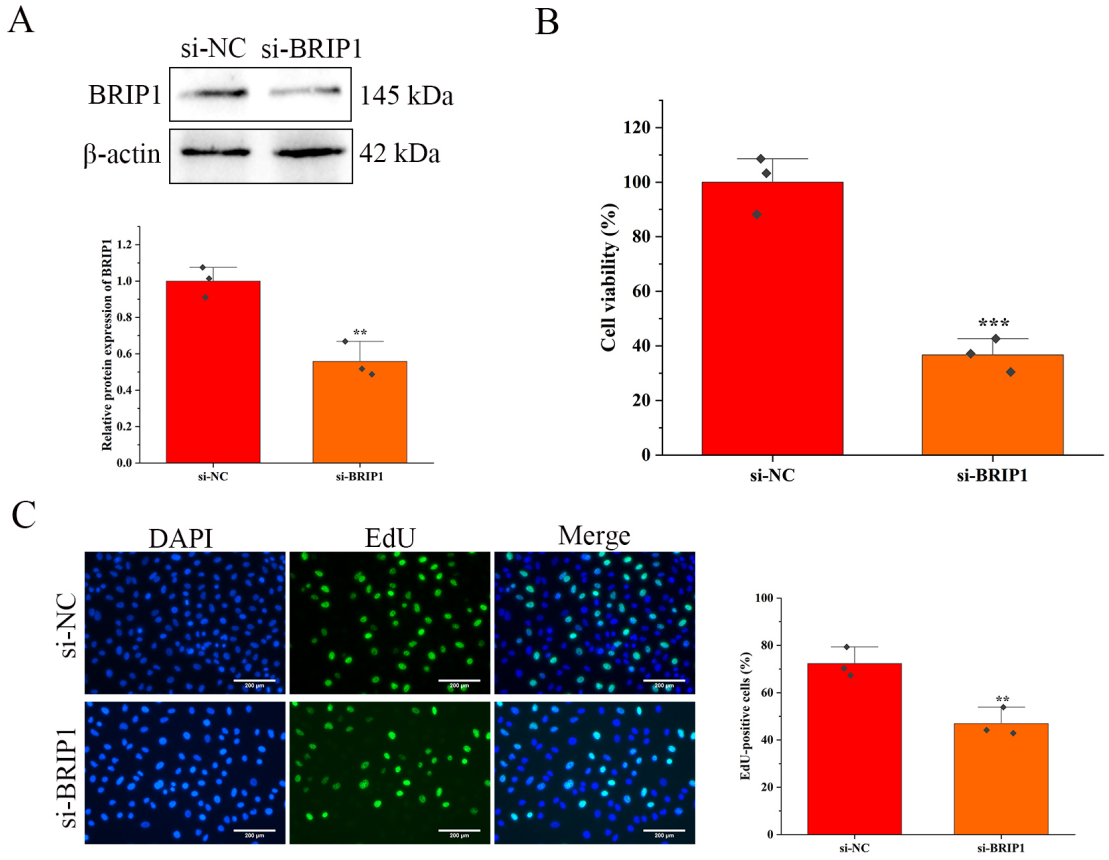

Fig. 2. Effects of down-regulation of *BRIP1* on cell viability and proliferation in U251 cells. (A) Verification of transfection efficiency by qRT-PCR analysis of *BRIP1* expression in U251 cells transfected with si-NC (negative control) or si-*BRIP1*, n = 3. (B) Cell viability was assessed using the Cell counting kit-8 (CCK-8) assay, n = 3. (C) Cell proliferation was evaluated using the 5-Ethynyl-2′-deoxyuridine (EdU) assay, 200×, n = 3. ** $p < 0.01$, *** $p < 0.001$.

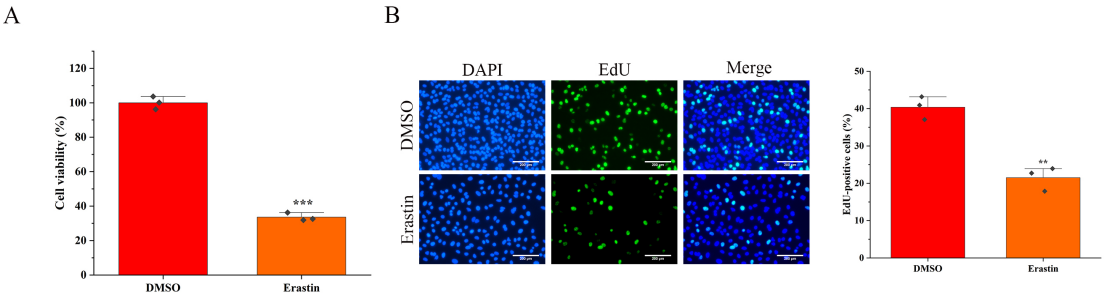

Fig. 3. Effects of erastin on cell viability and proliferation in U251 cells. (A) Cell viability was assessed using the CCK-8 assay after treatment with erastin, n = 3. (B) Cell proliferation was evaluated using the EdU assay after erastin treatment, 200×, n = 3. ** $p < 0.01$, *** $p < 0.001$.

Discussion

Gliomas are a significant health concern all around the world [23]. Gliomas are a common type of primary brain tumor in the United States, comprising around 27% of all diagnosed primary brain and central nervous system tumors in both adults and children, according to the Central Brain Tumor Registry of the United States (CBTRUS) [24]. Gliomas are also a significant health concern in China. According to the previous study, gliomas accounted for approximately 41.8% of all primary brain tumors in China between 2000 and 2010 [25]. Gliomas are known to involve complex interactions between genetic factors, environmental exposures, and cellular processes [26]. Various genetic alterations have been identified in gliomas, including mutations in genes such as isocitrate dehydrogenase (NADP(+)) 1 (*IDH1*), isocitrate dehydrogenase (NADP(+)) 2 (*IDH2*), tumor protein 53 (*TP53*), epidermal growth factor recep-

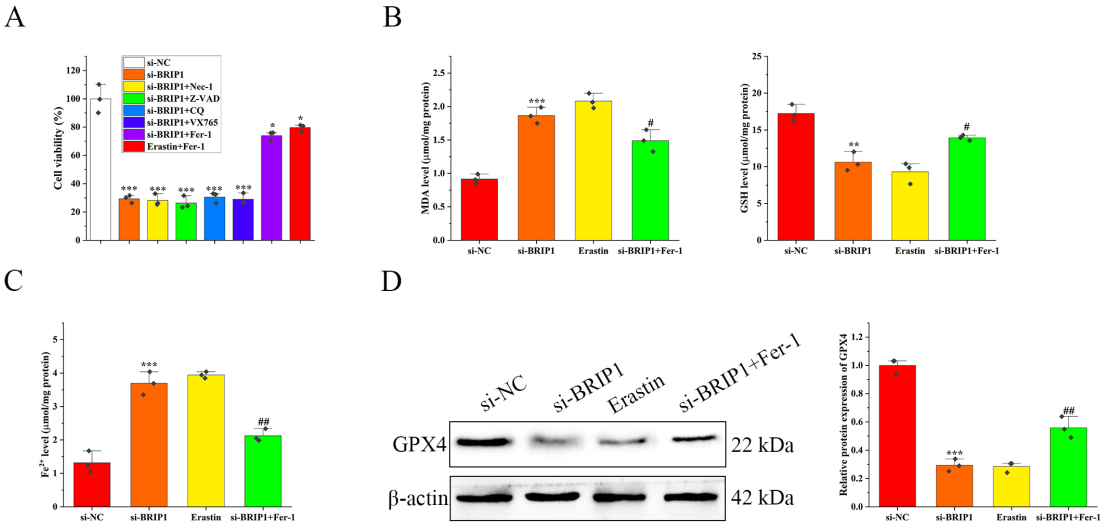

Fig. 4. Effects of down-regulation of *BRIP1* on ferroptosis in U251 cells. (A) Cell viability was assessed using the CCK-8 assay after treatment with various inhibitors in U251 cells transfected with si-*BRIP1*, n = 3. (B) The level of glutathione (GSH) and the content of malondialdehyde (MDA) were measured to assess ferroptosis-related changes in U251 cells, n = 3. (C) The content of Fe^{2+} was measured in U251 cells, n = 3. (D) The expression of Glutathione peroxidase 4 (*Gpx4*) was analyzed by Western blot, n = 3. Compared with si-NC group * $p < 0.05$, ** $p < 0.01$, *** $p < 0.001$, compared with si-*BRIP1* group $^{\#}$ $p < 0.05$, $^{\#\#}$ $p < 0.01$. Fer-1, ferrostain-1.

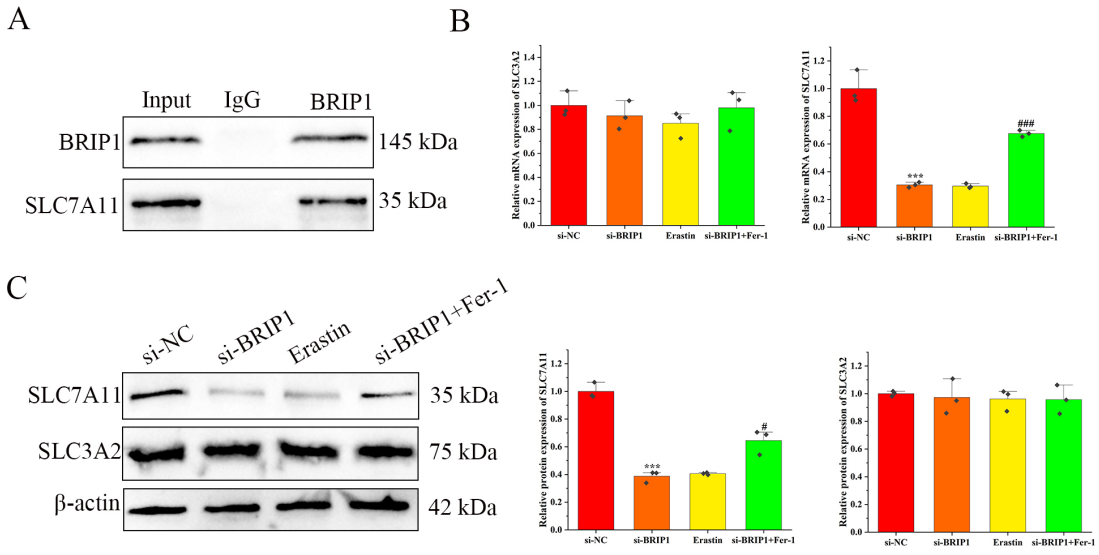

Fig. 5. Effects of down-regulation of *BRIP1* or treatment of erastin on the expression of Solute Carrier Family 7 Member 11 (*SLC7A11*) and Solute Carrier Family 3 Member 2 (*SLC3A2*) in U251 cells. (A) Co-immunoprecipitation (co-IP) for detection of BRIP1 binding to SLC7A11. (B) The mRNA expression levels of *SLC7A11* and *SLC3A2* were analyzed by qRT-PCR, n = 3. (C) The protein expression levels of *SLC7A11* and *SLC3A2* were analyzed by Western blot, n = 3. Compared with si-NC group *** $p < 0.001$, compared with si-*BRIP1* group $^{\#}$ $p < 0.05$, $^{\#\#\#}$ $p < 0.001$.

tor (*EGFR*), and others [27,28]. These mutations can disrupt cellular signaling pathways, promote uncontrolled cell growth, and contribute to tumor formation. However, the exact sequence of events and the precise mechanisms by which these genetic alterations lead to glioma development and progression are not yet completely clear.

Herein, we investigated the expression and functional role of *BRIP1* in glioma, specifically focusing on U251 cells. Our findings revealed that *BRIP1* level was significantly increased in glioma patients and cell lines, consistent with previous studies [29–31]. We observed the highest expression of *BRIP1* in U251 cells, which led us to select them as the *in vitro* model for further investigations.

To elucidate the functional significance of *BRIP1* in glioma, we down-regulated its expression using siRNA in U251 cells. Knocking down *BRIP1* led to a notable re-

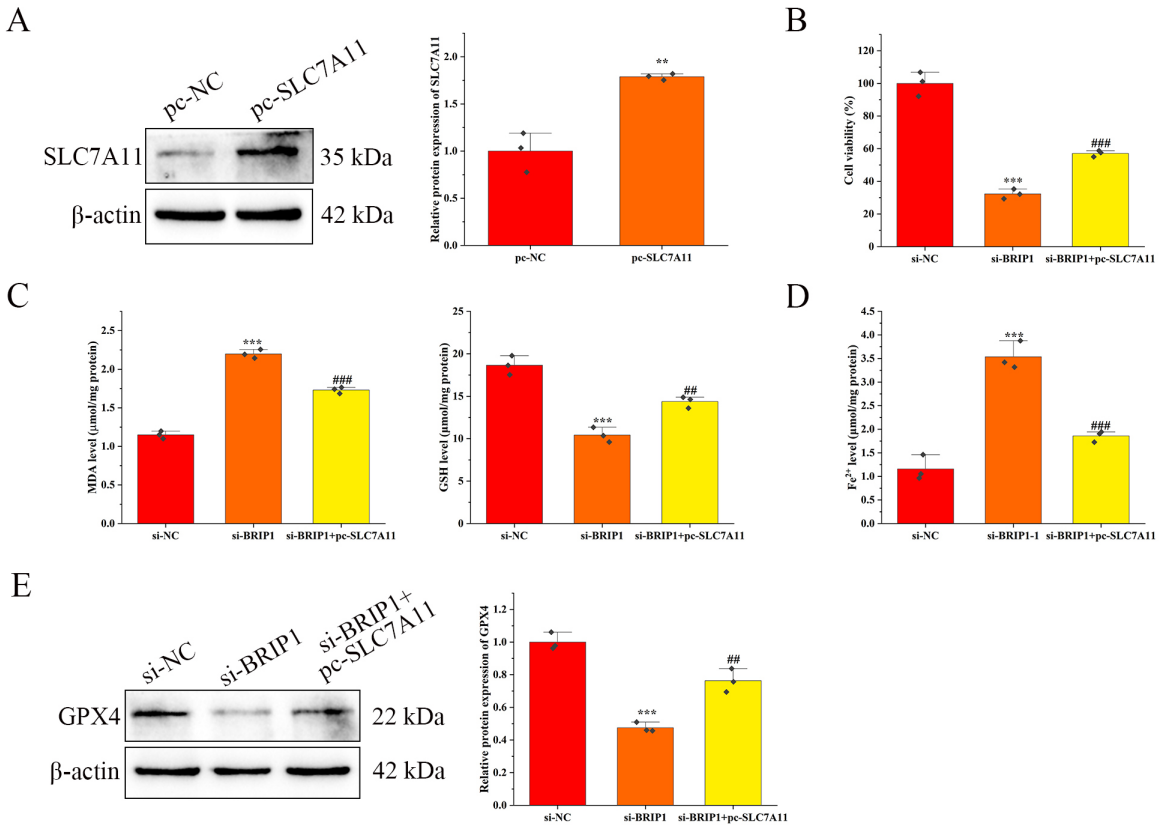

Fig. 6. Role of *SLC7A11* in the rescue experiment in si-*BRIP1*-treated U251 cells. (A) The expression of *SLC7A11* was analyzed by Western blot to verify the transfection efficiency after transfecting U251 cells with pc-NC or pc-*SLC7A11*, n = 3. (B) Cell viability was assessed using the CCK-8 assay to evaluate the rescue effect of pc-*SLC7A11*, n = 3. (C) The levels of MDA and GSH were measured to assess the rescue effect of pc-*SLC7A11*, n = 3. (D) The content of Fe^{2+} was measured to evaluate the rescue effect of pc-*SLC7A11*, n = 3. (E) The expression of *Gpx4* was analyzed by Western blot to assess the rescue effect of pc-*SLC7A11*, n = 3. Compared with pc-NC or si-NC group ** $p < 0.01$, *** $p < 0.001$, compared with si-*BRIP1* group $^{\#\#}$ $p < 0.01$, $^{\#\#\#}$ $p < 0.001$.

duction in cell viability and proliferation, suggesting its involvement in promoting the growth of glioma cells. These findings align with prior research indicating that down-regulation of *BRIP1* has shown similar effects in various cancer types [32].

Ferroptosis, a programmed cell death pathway characterized by lipid peroxidation and the accumulation of reactive oxygen species (ROS) dependent on iron, has gained significant attention as a crucial process in cancer biology [33]. To explore the involvement of ferroptosis in glioma cells, we treated U251 cells with erastin, a ferroptosis activator. Remarkably, erastin treatment led to a significant decrease in cell viability and proliferation, mirroring the effects of *BRIP1* down-regulation, which suggests that si-*BRIP1* may activate ferroptosis in U251 cells, similar to the effects of erastin treatment.

To further study the mode of programmed cell death induced by si-*BRIP1*, we performed additional experiments. We found that cell viability was not affected by various inhibitors of apoptosis or autophagy in si-*BRIP1*-treated cells. However, the addition of Fer-1, a ferroptosis inhibitor, increased cell viability, indicating that si-*BRIP1* might promote ferroptosis in U251 cells. Consistent with this, we observed increased levels of malondialdehyde (MDA) and Fe^{2+} content, as well as decreased glutathione (GSH) activity in si-*BRIP1* or erastin-treated cells. These changes were reversed by Fer-1, further supporting the activation of ferroptosis in si-*BRIP1*-treated glioma cells. Additionally, the down-regulation of *BRIP1* or erastin treatment resulted in decreased expression of *Gpx4*, a key regulator of ferroptosis, which was rescued by Fer-1.

We also analyzed the expression of *SLC7A11* and *SLC3A2*, two genes involved in ferroptosis regulation [34]. Interestingly, *SLC7A11* expression was reduced in si-*BRIP1* or erastin-treated cells, while *SLC3A2* expression showed no significant difference among the experimental groups. The reduction in *SLC7A11* expression was reversed by Fer-1 specifically in si-*BRIP1*-treated cells. These findings suggest that *SLC7A11* may play a role in the downstream effects of *BRIP1* in glioma cells, potentially contributing to the activation of ferroptosis.

To validate the involvement of *SLC7A11*, a rescue experiment was conducted by overexpressing *SLC7A11* in si-*BRIP1*-treated U251 cells. Remarkably, the overexpression

of *SLC7A11* effectively reversed the negative effects induced by si-*BRIP1*, including the reduction in cell viability, the increase in MDA levels, the decrease in GSH activity, the elevation of Fe^{2+} content, and the down-regulation of *Gpx4*. These results provide further support for the role of *SLC7A11* in mediating the effects of *BRIP1* on ferroptosis-related processes in glioma cells.

In conclusion, our study suggests that *BRIP1* is able to influence the biological process of glioma cells by regulating iron death. However, it is worth reflecting here that we did not deeply investigate the relationship between *BRIP1* and other types of programmed cell death, which is a limitation of this study, and thus this is a direction we need to follow up with in-depth research. In addition, we should collect relevant information about clinical patients, including prognosis, survival rate, etc., and analyze their relationship with *BRIP1*, so as to improve the diagnosis and treatment of gliomas in the clinic.

Conclusion

The present study has primarily been carried out at the cell line level, and it lacks the inclusion of *in vivo* mouse study content and primary cell-related study content, which are crucial for our follow-up research programme. However, our study demonstrated that *BRIP1* was upregulated in glioma patients and cell lines. Downregulation of *BRIP1* activated the iron metabolic response in U251 cells, as evidenced by changes in cell viability, proliferation, lipid peroxidation, iron levels, and *Gpx4* expression. In addition, *SLC7A11* expression appeared to be involved in the downstream effects of *BRIP1*. These findings provide valuable insights into the potential role of *BRIP1* and iron oxidation in glioma progression, suggesting that targeting *BRIP1* and iron oxidation-associated pathways may have therapeutic implications for glioma treatment.

Availability of Data and Materials

The datasets used and/or analyzed during the current study are available from the corresponding author on reasonable request.

Author Contributions

CC designed the research study. ZW performed the research. JS and XL provided help and advice on the experiments. CC and ZW analyzed the data. CC wrote the first draft. All authors contributed significantly to editorial changes of important content. All authors read and approved the final manuscript. All authors have participated sufficiently in the work and agreed to be accountable for all aspects of the work.

Ethics Approval and Consent to Participate

Not applicable.

Acknowledgment

Not applicable.

Funding

This research received no external funding.

Conflict of Interest

The authors declare no conflict of interest.

References

[1] Zhang L, Wang L, Xia H, Tan Y, Li C, Fang C. Connectomic mapping of brain-spinal cord neural networks: Future directions in assessing spinal cord injury at rest. Neuroscience Research. 2022; 176: 9–17.

[2] Perry A, Wesseling P. Histologic classification of gliomas. Handbook of Clinical Neurology. 2016; 134: 71–95.

[3] Omuro A, DeAngelis LM. Glioblastoma and other malignant gliomas: a clinical review. JAMA. 2013; 310: 1842–1850.

[4] Prakash O, Lukiw WJ, Peruzzi F, Reiss K, Musto AE. Gliomas and seizures. Medical Hypotheses. 2012; 79: 622–626.

[5] Davis ME. Epidemiology and Overview of Gliomas. Seminars in Oncology Nursing. 2018; 34: 420–429.

[6] Zhu J, Xu Y, Lu XJ. Stereotactic Body Radiation Therapy and Ablative Therapies for Solid Tumors: Recent Advances and Clinical Applications. Technology in Cancer Research & Treatment. 2019; 18: 1533033819830720.

[7] Liu J, Hong M, Li Y, Chen D, Wu Y, Hu Y. Programmed Cell Death Tunes Tumor Immunity. Frontiers in Immunology. 2022; 13: 847345.

[8] Hirayama D, Iida T, Nakase H. The Phagocytic Function of Macrophage-Enforcing Innate Immunity and Tissue Homeostasis. International Journal of Molecular Sciences. 2017; 19: 92.

[9] Gao W, Wang X, Zhou Y, Wang X, Yu Y. Autophagy, ferroptosis, pyroptosis, and necroptosis in tumor immunotherapy. Signal Transduction and Targeted Therapy. 2022; 7: 196.

[10] Yang WS, Stockwell BR. Ferroptosis: Death by Lipid Peroxidation. Trends in Cell Biology. 2016; 26: 165–176.

[11] Bersuker K, Hendricks JM, Li Z, Magtanong L, Ford B, Tang PH, *et al*. The CoQ oxidoreductase FSP1 acts parallel to GPX4 to inhibit ferroptosis. Nature. 2019; 575: 688–692.

[12] Liu T, Zhu C, Chen X, Guan G, Zou C, Shen S, *et al*. Ferroptosis, as the most enriched programmed cell death process in glioma, induces immunosuppression and immunotherapy resistance. Neuro-oncology. 2022; 24: 1113–1125.

[13] Shi J, Yang N, Han M, Qiu C. Emerging roles of ferroptosis in glioma. Frontiers in Oncology. 2022; 12: 993316.

[14] Wan RJ, Peng W, Xia QX, Zhou HH, Mao XY. Ferroptosis-related gene signature predicts prognosis and immunotherapy in glioma. CNS Neuroscience & Therapeutics. 2021; 27: 973–986.

[15] Moyer CL, Ivanovich J, Gillespie JL, Doberstein R, Radke MR, Richardson ME, *et al*. Rare *BRIP1* Missense Alleles Confer Risk for Ovarian and Breast Cancer. Cancer Research. 2020; 80: 857–867.

[16] Stadler ZK, Maio A, Chakravarty D, Kemel Y, Sheehan M, Salo-Mullen E, *et al*. Therapeutic Implications of Germline Testing in Patients With Advanced Cancers. Journal of Clinical Oncology:

Official Journal of the American Society of Clinical Oncology. 2021; 39: 2698–2709.

[17] Monteiro LJ, Khongkow P, Kongsema M, Morris JR, Man C, Weekes D, *et al*. The Forkhead Box M1 protein regulates BRIP1 expression and DNA damage repair in epirubicin treatment. Oncogene. 2013; 32: 4634–4645.

[18] Koppula P, Zhuang L, Gan B. Cystine transporter SLC7A11/xCT in cancer: ferroptosis, nutrient dependency, and cancer therapy. Protein & Cell. 2021; 12: 599–620.

[19] Yuan S, Wei C, Liu G, Zhang L, Li J, Li L, *et al*. Sorafenib attenuates liver fibrosis by triggering hepatic stellate cell ferroptosis via HIF-1α/SLC7A11 pathway. Cell Proliferation. 2022; 55: e13158.

[20] Fu C, Wu Y, Liu S, Luo C, Lu Y, Liu M, *et al*. Rehmannioside A improves cognitive impairment and alleviates ferroptosis via activating PI3K/AKT/Nrf2 and SLC7A11/GPX4 signaling pathway after ischemia. Journal of Ethnopharmacology. 2022; 289: 115021.

[21] Park JW, Kilic O, Deo M, Jimenez-Cowell K, Demirdizen E, Kim H, *et al*. CIC reduces xCT/SLC7A11 expression and glutamate release in glioma. Acta Neuropathologica Communications. 2023; 11: 13.

[22] Sun S, Guo C, Gao T, Ma D, Su X, Pang Q, *et al*. Hypoxia Enhances Glioma Resistance to Sulfasalazine-Induced Ferroptosis by Upregulating SLC7A11 via PI3K/AKT/HIF-1α Axis. Oxidative Medicine and Cellular Longevity. 2022; 2022: 7862430.

[23] McNamara C, Mankad K, Thust S, Dixon L, Limback-Stanic C, D'Arco F, *et al*. 2021 WHO classification of tumours of the central nervous system: a review for the neuroradiologist. Neuroradiology. 2022; 64: 1919–1950.

[24] Ostrom QT, Price M, Neff C, Cioffi G, Waite KA, Kruchko C, *et al*. CBTRUS Statistical Report: Primary Brain and Other Central Nervous System Tumors Diagnosed in the United States in 2015-2019. Neuro-oncology. 2022; 24: v1–v95.

[25] Shen F, Wu CX, Yao Y, Peng P, Qin ZY, Wang Y, *et al*. Transition over 35 years in the incidence rates of primary central nervous system tumors in Shanghai, China and histological subtyping based on a single center experience spanning 60 years. Asian Pacific Journal of Cancer Prevention: APJCP. 2013; 14: 7385–7393.

[26] Liu X, Yang J, Li H, Wang Q, Yu Y, Sun X, *et al*. Quantifying substantial carcinogenesis of genetic and environmental factors from measurement error in the number of stem cell divisions. BMC Cancer. 2022; 22: 1194.

[27] Zou P, Xu H, Chen P, Yan Q, Zhao L, Zhao P, *et al*. IDH1/IDH2 mutations define the prognosis and molecular profiles of patients with gliomas: a meta-analysis. PloS One. 2013; 8: e68782.

[28] Alentorn A, Labussière M, Sanson M, Delattre JY, Hoang-Xuan K, Idbaih A. Genetics and brain gliomas. Presse Medicale (Paris, France: 1983). 2013; 42: 806–813.

[29] de Sousa JF, Torrieri R, Serafim RB, Di Cristofaro LFM, Escanfella FD, Ribeiro R, *et al*. Expression signatures of DNA repair genes correlate with survival prognosis of astrocytoma patients. Tumour Biology: the Journal of the International Society for Oncodevelopmental Biology and Medicine. 2017; 39: 1010428317694552.

[30] Yu Y, Liang Z, Song X, Fu W, Xu J, Lei Y, *et al*. BRAHMA-interacting proteins BRIP1 and BRIP2 are core subunits of Arabidopsis SWI/SNF complexes. Nature Plants. 2020; 6: 996–1007.

[31] Katheeja MN, Das SP, Das R, Laha S. BRCA1 interactors, RAD50 and BRIP1, as prognostic markers for triple-negative breast cancer severity. Frontiers in Genetics. 2023; 14: 1035052.

[32] Rizeq B, Sif S, Nasrallah GK, Ouhtit A. Novel role of BRCA1 interacting C-terminal helicase 1 (BRIP1) in breast tumour cell invasion. Journal of Cellular and Molecular Medicine. 2020; 24: 11477–11488.

[33] Chen X, Kang R, Kroemer G, Tang D. Broadening horizons: the role of ferroptosis in cancer. Nature Reviews. Clinical Oncology. 2021; 18: 280–296.

[34] Tan H, Chen J, Li Y, Li Y, Zhong Y, Li G, *et al*. Glabridin, a bioactive component of licorice, ameliorates diabetic nephropathy by regulating ferroptosis and the VEGF/Akt/ERK pathways. Molecular Medicine (Cambridge, Mass.). 2022; 28: 58.